PHILOSOPHICAL TRANSACTIONS OF THE ROYAL SOCIETY A MATHEMATICAL, PHYSICAL & ENGINEERING SCIENCES

Numerical Solutions of the Kinematic Dynamo Problem

D. Gubbins

Phil. Trans. R. Soc. Lond. A 1973 **274**, 493-521
doi: 10.1098/rsta.1973.0074

NUMERICAL SOLUTIONS OF THE KINEMATIC DYNAMO PROBLEM

By D. GUBBINS†

Department of Geodesy and Geophysics, Madingley Rise, Madingley Road, Cambridge, England

(*Communicated by Sir Edward Bullard, F.R.S. – Received 4 December* 1972)

CONTENTS

The expansion method of Bullard & Gellman is used to find numerical solutions of the induction equation in a sphere of conducting fluid. Modifications are made to the numerical methods, and one change due to G. O. Roberts greatly increases the efficiency of the scheme. Calculations performed recently by Lilley are re-examined. His solutions, which appeared to be convergent, are shown to diverge when a higher level of truncation is used. Other similar dynamo models are investigated and it is found that these also do not provide satisfactory steady solutions for the magnetic field.

Axially symmetric motions which depend on spherical harmonics of degree n are examined. Growing solutions, varying with longitude, ϕ, as $e^{i\phi}$, are found for the magnetic field, and numerical convergence of the solutions is established. The field is predominantly an equatorial dipole with a toroidal field symmetric about the same axis. When n is large the problem lends itself to a two-scale analysis. Comparisons are made between the approximate results of the two-scale method and the numerical results. There is agreement when n is large. When n is small the efficiency of the dynamo is lowered. It is shown that the dominant effect of a large microscale magnetic Reynolds number is the expulsion of magnetic flux by eddies to give a rope-like structure for part of the field. Physical interpretations are given which explain the dynamo action of these motions, and of related flows which support rotating magnetic fields.

1. Introduction

The dynamo problem can be stated: 'Can a body of homogeneous conducting fluid maintain a magnetic field indefinitely against resistive losses?' It is widely believed that the Earth's magnetic field is maintained by some dynamo mechanism acting in the highly conducting liquid core. There are other examples of dynamos in astrophysics; the sun possesses a magnetic field which is known quite accurately as a function of space and time, and E. N. Parker (1971) has attempted to explain the galactic magnetic field by means of a dynamo mechanism.

This paper is concerned only with the kinematic dynamo problem. In this the fluid velocity, $\boldsymbol{u}$, is specified and one calculates the resulting magnetic field, ignoring the back-reaction of the Lorentz force on the fluid flow.

† Now at Cooperative Institute for Research in Environmental Sciences, University of Colorado/National Oceanic and Atmospheric Administration, Boulder, Colorado 80302, U.S.A.

With the usual assumptions (P. H. Roberts 1967), Maxwell's equations give the induction equation:

$$\partial \boldsymbol{B}/\partial t = \operatorname{curl}(\boldsymbol{u} \times \boldsymbol{B}) + \lambda \nabla^2 \boldsymbol{B} \tag{1.1}$$

and

$$\operatorname{div} \boldsymbol{B} = 0, \tag{1.2}$$

where $\lambda = (\mu\kappa)^{-1}$, $\boldsymbol{B}$ is the magnetic field, κ the electrical conductivity and μ the permeability. It is assumed that μ and κ are uniform throughout the fluid. If $\boldsymbol{u}$ is prescribed, then (1.1) is linear in $\boldsymbol{B}$.

Let $\mathscr{U}$ and $\mathscr{L}$ be typical values of $\boldsymbol{u}$ and $\boldsymbol{r}$. Scaling t with $(\mathscr{L}^2\mu\kappa)^{-1}$, the diffusive time scale, (1.1) becomes

$$\partial \boldsymbol{B}/\partial t = R_{\mathrm{m}} \operatorname{curl}(\boldsymbol{u} \times \boldsymbol{B}) + \nabla^2 B, \tag{1.3}$$

where $R_{\mathrm{m}} = \mathscr{U}\mathscr{L}\mu\kappa$, the magnetic Reynolds number.

The problem of most astrophysical and geophysical interest is when the conducting fluid is contained in a sphere surrounded by an insulator. All components of $\boldsymbol{B}$ must be continuous across the bounding surface of the conductor, and there can be no sources of field in the insulator or at infinity. The last condition reduces to

$$|\boldsymbol{B}| = O(r^{-3}) \quad \text{as} \quad r \to \infty,$$

where the origin of coordinates is inside the conductor.

Cowling (1934) proved that an axially symmetric field cannot be maintained by any velocity. Later, however, Backus (1958) and Herzenberg (1958) gave analytic proofs that fluid motions could support magnetic fields. The general investigation of the dynamo action of fluid motions is a very complicated problem, and the only practicable method is to solve the equations numerically on a computer. Elsasser (1946*a*, *b*, 1947), Bullard & Gellman (1954) and E. N. Parker (1955) pioneered work on the dynamics of the core and on physical ideas of dynamo action. Numerical solutions were attempted by Bullard & Gellman, and although they obtained evidence of a convergent, steady solution, the recent work of Gibson, P. H. Roberts & Scott (1969) and Lilley (1970) has shown that their solution does not converge when a more accurate representation is taken for the field.

Braginskiĭ (1965) considered large magnetic Reynolds number dynamos with velocities and magnetic fields which are almost axially symmetric, and found that the Bullard–Gellman dynamo could not be expected to support such a field in the limit:

$$R_{\mathrm{m}} \to \infty, \quad \nu R_{\mathrm{m}}^{\frac{1}{2}} \to \text{finite limit},$$

where ν is the ratio of (asymmetric) poloidal motion to (symmetric) toroidal motion. Tough (1967) extended the analysis to the next order in $R_{\mathrm{m}}^{-\frac{1}{2}}$ (see also Soward 1971, 1972). D. I. Black (1969, personal communication) proved that both these statements apply to any velocity with the symmetry

$$\boldsymbol{u}'_{\mathrm{p}}(\phi) = -\boldsymbol{u}'_{\mathrm{p}}(-\phi) \tag{1.4}$$

for some choice of axes, where ϕ is the third spherical coordinate and $\boldsymbol{u}'_{\mathrm{p}}$ the meridional part of the non-axially symmetric velocity. Lilley (1970) modified the Bullard–Gellman motion by adding an extra term to $\boldsymbol{u}'$ to remove the symmetry of (1.4), and obtained results which were, although not entirely convincing, much better than those using the original motion.

It is possible to obtain approximate solutions to the kinematic problem by the multiple scale method (Steenbeck, Krause & Rädler 1966). The field is separated into large and small scale parts:

$$\boldsymbol{B} = \boldsymbol{B}_0 + \boldsymbol{B}'.$$

The solution is particularly simple when the microscale magnetic Reynolds number is small. Making the assumptions

$$|\boldsymbol{B}'| \ll |\boldsymbol{B}_0|,$$

$$|\nabla^2 \boldsymbol{B}'| \simeq |\nabla^2 \boldsymbol{B}_0| \simeq |\boldsymbol{B}_0|,$$

$$\lambda |\boldsymbol{B}'| \simeq |\boldsymbol{B}_0|,$$

the induction equation gives

$$\frac{\partial \boldsymbol{B}_0}{\partial t} = \operatorname{curl} (\overline{\boldsymbol{u} \times \boldsymbol{B}'}) + \lambda \nabla^2 \boldsymbol{B}_0, \tag{1.5}$$

$$(\boldsymbol{B}_0 . \nabla) \boldsymbol{u} \approx \lambda \nabla^2 \boldsymbol{B}', \tag{1.6}$$

where the overbar denotes an average over a spatial extent large compared with the small scale, and small compared with the large scale. These equations are much easier to solve than the full induction equation.

This method has been used in a study of turbulence (Steenbeck *et al.* 1966; Moffatt 1970) and is related to the theory of periodic dynamos (G. O. Roberts 1970). For homogeneous, pseudo-isotropic turbulence the e.m.f. $\overline{\boldsymbol{u} \times \boldsymbol{B}'}$ has the form $\alpha \boldsymbol{B}_0$, where α is related to $\overline{\boldsymbol{u} . \operatorname{curl} \boldsymbol{u}}$, which has been called the 'helicity' by Moffatt (1970). This production of current parallel to the mean field is called the α-effect. The equation for the mean field is

$$\partial \boldsymbol{B}_0 / \partial t = R_{\mathrm{m}} \operatorname{curl} (\boldsymbol{u}_0 \times \boldsymbol{B}_0 + \alpha \boldsymbol{B}_0) + \nabla^2 \boldsymbol{B}_0. \tag{1.7}$$

This equation has been solved numerically in a sphere by Braginskiĭ (1964), Krause & Steenbeck (1967), Steenbeck & Krause (1969*a*, *b*), P. H. Roberts (1971) and P. H. Roberts & Stix (1972). The work supports the view that a large-scale field can be maintained by the α-effect.

G. O. Roberts has investigated a class of spherical dynamos by solving the full induction equation numerically (P. H. Roberts in Zmuda 1971). A grid-point method was used for the solution; it is the first demonstration of dynamo action in a sphere that has been accomplished numerically. It is this result that dictated the choice of motions for the numerical work described in § 3.

The numerical method used in this paper is essentially the same as that of Bullard & Gellman (1954). The induction equation is replaced by a set of ordinary differential equations by expanding the velocity and magnetic field in vector spherical harmonics:

$$\boldsymbol{T} = \left\{0; \quad \frac{T(r)}{r \sin\theta} \frac{\partial Y}{\partial \phi}; \quad -\frac{T(r)}{r} \frac{\partial Y}{\partial \theta}\right\},$$

$$\boldsymbol{S} = \left\{\frac{n(n+1)}{r^2} S(r) Y; \quad \frac{1}{r} \frac{\partial S}{\partial r} \frac{\partial Y}{\partial \theta}; \quad \frac{1}{r \sin\theta} \frac{\partial S}{\partial r} \frac{\partial Y}{\partial \phi}\right\},$$

where (r, θ, ϕ) are the spherical coordinates, Y denotes the harmonic:

$$Y_n^{m\{c\}}(\theta, \phi) = P_n^m(\cos\theta) \begin{Bmatrix} \cos \\ \sin \end{Bmatrix} m\phi$$

and P_n^m is a Legendre function with the usual (Ferrer) normalization. The properties of $\boldsymbol{S}$ and $\boldsymbol{T}$ are summarized in Bullard & Gellman. The differential equations resulting from the induction equation are

$$r^2 \frac{\partial S_\gamma}{\partial t} - r^2 \frac{\partial^2 S_\gamma}{\partial r^2} + \gamma(\gamma+1) S_\gamma = R_{\mathrm{m}} \sum_{\alpha, \beta} (S_\alpha S_\beta S_\gamma) + (T_\alpha T_\beta S_\gamma) + (S_\alpha T_\beta S_\gamma) \tag{1.8}$$

and a similar equation for T_γ, where α, β and γ are blanket labels representing u, m, c and s. The quantities in brackets are called interaction terms. For example $(S_\alpha S_\beta S_\gamma)$ represents the production of S_γ field from S_β field by the S_α velocity. They are given explicitly in Bullard & Gellman (1954, eqn. 24) and depend on the Gaunt and Elsasser integrals (Albasing, Bell & Cooper 1963; Gibson *et al.* 1969; James 1972).

If certain selection rules are not obeyed, the Gaunt or Elsasser integrals vanish, and consequently only some field harmonics are related by a specific velocity harmonic. The selection rules can be applied systematically and relate the various terms in the expansion for $\boldsymbol{B}$. The resulting interaction diagrams are very instructive in understanding how the dynamo works. Sometimes the interaction diagram for a particular choice of motion splits into completely unrelated parts. For example, if $\boldsymbol{u}$ is axially symmetric, m_α is zero and the relevant integrals are zero unless $m_\beta = m_\gamma$ (selection rules 1(*c*) and 2(*c*), Bullard & Gellman). This means there is a set of interaction diagrams, one for each value of m_γ, and solutions for the field exist which are dependent only on $\cos m_\gamma \phi$ or $\sin m_\gamma \phi$.

Sometimes it is expedient to use complex harmonics, defined by

$$Y_n^m(\theta, \phi) = P_n^m(\cos\theta)\, \mathrm{e}^{\mathrm{i}m\phi}.$$

The selection rules are modified; for axially symmetric $\boldsymbol{u}$ rules **1(*c*)**, **1**(*d*), 2(*c*), 2(*d*) and 2(*e*) are replaced by the condition:

$$m_\beta = m_\gamma.$$

In §2 steady fields are sought. However, steady solutions of the dynamo problem may not always exist. A solution to the time-dependent problem is more likely to yield meaningful results than a search for a steady solution in which R_m is calculated, and for the solutions in §§3 and 4 we write the time dependence of $\boldsymbol{B}$ in the form:

$$\boldsymbol{B} = \mathrm{Re}\, \tilde{\boldsymbol{B}}\, \mathrm{e}^{pt}$$

with p complex. This leads to the equation:

$$p\tilde{\boldsymbol{B}} = \mathrm{R_m\, curl}\, (\boldsymbol{u} \times \tilde{\boldsymbol{B}}) + \nabla^2 \tilde{\boldsymbol{B}},$$

R_m is chosen and p found as an eigenvalue. When R_m is zero this equation becomes the vector diffusion equation, which has an analytical solution. The slowest decaying mode in a sphere is a dipolar field based on the spherical Bessel function $rj_1(\pi r)$. The decay rate is $-\pi^2$. This solution was used to check the numerical work. By increasing R_m from zero, it is usually possible to follow the decay rate away from this analytical value, and the real part of p will become positive for a functioning dynamo. As R_m increases, one expects the field to become more complicated (or small scale), because large magnetic Reynolds numbers do not suppress small-scale fields. Such fields will be more difficult to represent numerically and the rounding errors increase (see below). By increasing R_m from zero it should be possible to detect the point at which the numerical solution becomes unreliable.

The numerical solution is effected by truncating the series for $\boldsymbol{u}$ and $\boldsymbol{B}$ at some point and using first-order finite difference formulae for the radial derivatives. This yields an algebraic eigenvalue problem with a banded matrix, with R_m or p as eigenvalue. The eigenvalue nearest to some chosen initial value is found by the inverse iteration method (Isaacson & Keller 1966). The procedure for using the inverse iteration method with banded matrices is described in detail by

Wilkinson (1965), but for the present problem we use a modification due to G. O. Roberts (1972), in which the matrix inversion is performed without interchange of columns. This method retains the banded structure of the matrices, but rounding errors are liable to be large, particularly when the magnetic Reynolds number is large.

The advantages of the inverse iteration method over the QR algorithm used by Lilley are a factor of $\frac{1}{4}n_r$ in storage, where n_r is the number of radial grid points, and a factor of $8n_r^2$ in time even if only one of the eigenvectors is found by means of the QR algorithm. The savings in time are enormous in any case, for one of the calculations in §3 by a factor of 10^5.

The solution of the eigenvalue problem yields the magnetic field (eigenvector) as well as the magnetic Reynolds number or the growth rate (eigenvalue), depending on whether a steady or a time-dependent solution is sought. The eigenvector contains all the available information about the mechanism maintaining the field. If the solution decays, the structure can sometimes show why it decays. It is therefore very desirable to examine the field for any solution. In many numerical studies the field which is maintained is not discussed, presumably because of the difficulty of presenting it in a concise way. A further reason for studying the eigenvector is to test convergence of the solution. It is usual to test convergence by looking at the change in the eigenvalue when the degree of truncation of the harmonic series and the number of grid points are increased (Lilley 1970; Gibson & Roberts 1969). R. L. Parker (1969, private communication) has suggested that the harmonics that are neglected because of the truncation of the field series may be estimated individually by perturbation theory. The theory may be applied to the eigenvalue problem of Bullard & Gellman for which the matrices are sparse but not banded. When the number of harmonics, representing the field is increased, the first and second order changes to the eigenvalue and eigenvector can be calculated explicitly (Gubbins 1972). An interesting result is that the only changes in the solution to first order in the neglected terms in the matrices are those in the new harmonics that enter because of the higher degree of truncation. The first-order change in the eigenvalue is zero. A similar result has been pointed out by Gibson & Roberts (1967). The fluctuations in the eigenvalue are therefore a very poor test of convergence of the numerical work, and a much better test is to look at the magnitudes of the highest harmonics in the eigenvector. Perturbation theory could also be used to find approximate values for the higher harmonics.

2. Lilley's dynamo and other Bullard–Gellman dynamos

This work was originally intended to be an extension of that of Lilley (1970). Although his results were not entirely convincing, it seemed likely that the calculations could be made to converge if better computing methods were used. The calculations do not converge, as is shown very clearly in this section. The results described in this section are entirely negative, but they are important in outlining the numerous difficulties involved, and it was these failures that prompted the approach of §§3 and 4.

Lilley (1970) chose the velocity: $\boldsymbol{u} = \boldsymbol{T}_1^0 + \boldsymbol{S}_2^{2c} + \boldsymbol{S}_2^{2s}$,

where the vector harmonics are based on the radial functions:

$$\left.\begin{aligned} T_1(r) &= 10r^2(1-r^2) \\ S_2^{2c}(r) &= r^3(1-r^2)^2 \\ S_2^{2s}(r) &= 1.6r^3(1-4r^2)^2 \quad \text{if} \quad r < 0.5 \\ &= 0 \quad\quad\quad\quad\quad\quad\ \text{if} \quad r \geqslant 0.5 \end{aligned}\right\} \tag{2.1}$$

This motion is the same as that of Bullard & Gellman with an extra $\boldsymbol{S}_2^{2s}$ term added to destroy the symmetry of equation (1.4). Some care is needed in the choice of the extra $S_2^{2s}(r)$ radial function. For example if the radial functions for the $\boldsymbol{S}_2^{2c}$ and $\boldsymbol{S}_2^{2s}$ harmonics are the same or multiples of each other, the plane of antisymmetry (equation 1.4) is only rotated by the addition of $\boldsymbol{S}_2^{2s}$ and not destroyed.

Lack of computer time and storage restricted Lilley's calculation. With the inverse iteration method one can not only carry the calculations to a higher degree of accuracy, but also explore many more choices of the velocity. This is important because the difficulties in solving the induction equation arise out of insufficient knowledge for a suitable choice for $\boldsymbol{u}$.

The method of solution used here is to calculate the R_m required for a steady state. The most unstable mode is that corresponding to the smallest real value of R_m. The inverse iteration method can be made to avoid complex roots simply by using real arithmetic. A rough estimate of the required eigenvalue has always been known in advance, and this was used to start the iteration. It is a simple matter to ensure that the eigenvalue found is the largest real one by starting the iteration from some very large real number.

TABLE 1. EIGENVALUES FOR LILLEY'S DYNAMO

l is the maximum allowed degree of the harmonics and n_r is the number of grid points used.

	$n_r = 10$	12	14	16	18	20	22	24	26	30	32
$l = 2$	22.7	—	—	—	—	—	—	—	26.0	—	—
3	12.2	—	—	22.3	—	—	—	—	39.9	—	—
4	11.5	13.7	—	—	19.5	21.1 (21.2)	22.6	23.9	25.0	—	—
5	12.7	15.5	18.4	21.3 (21.3)	24.1	27.1	30.2	33.6	37.5	48.3	No solution
6	—	—	—	20.9	—	—	—	—	—	—	—

Table 1 contains the eigenvalues found for Lilley's dynamo by the inverse iteration method. These results can be compared with Lilley's to check the accuracy. In fact there are some small differences because of some minor errors in Lilley's computer program, but the discrepancies are not significant. Apart from these differences, the values above and to the left of the solid line agree with Lilley's results. The numbers in parentheses were computed using double precision to check the rounding errors. Despite fears to the contrary, the rounding errors are not severe. The most significant part of this table is the $l = 5$ line. Along this row, as more grid points are used in the radial direction, the second differences are more than doubling at each step. For 32 radial divisions the method failed to converge on any real eigenvalue between 0 and 600. Clearly this is not a convergent solution. Poor convergence for this model has also been noted by P. H. Roberts (1972).

The magnetic field is shown in figure 1 at two truncation levels: $n_r = 16$, $l = 6$ and $n_r = 30$, $l = 5$. The first example is the case for which Lilley found the eigenvalue but not the eigenvector; the second solution demonstrates the spectacular divergence. Any solution to the induction equation may be multiplied by an arbitrary constant, and therefore in making comparisons such as that of figure 1 it is necessary to normalize the eigenvector in some way. Any choice of normalization will be arbitrary to a certain extent; the method used here is to make the sum of the absolute values of the components of the eigenvector $\boldsymbol{x}$ up to degree 5 proportional to the number of components. One could alternatively use the sum of squares of the components, or match the maximum values.

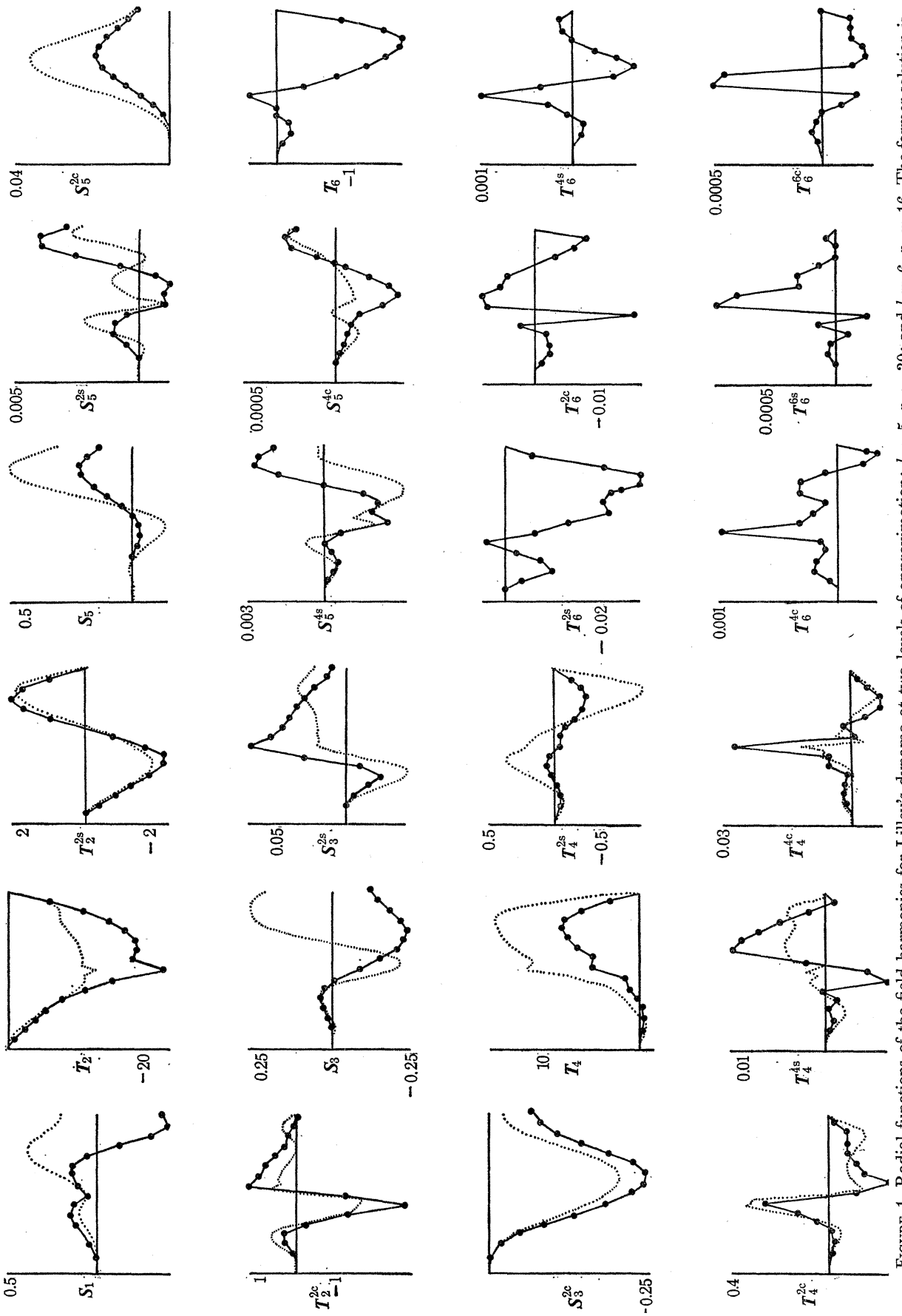

FIGURE 1. Radial functions of the field harmonics for Lilley's dynamo at two levels of approximation: $l = 5$, $n_r = 30$; and $l = 6$, $n_r = 16$. The former solution is plotted as dotted lines, the latter as solid lines with the value at each grid point marked.

It is also desirable to standardise the definition of magnetic Reynolds number. If it is based on the radius of the sphere and sup $|\boldsymbol{u}|$, all the values in table 1 must be multiplied by 2.86. This brings the typical value of the magnetic Reynolds number for Lilley's dynamo to nearer 50 than 20.

The eigenvectors in figure 1 have irregular behaviour near $r = 0.5$ because the components of the S_2^{2s} velocity have discontinuous derivatives there. The discontinuity in the S_2^{2s} velocity has been removed in the following three models by altering the radial functions of the harmonics.

Model 1

$$T_1(r) = 10r^2(1-r^2),$$
$$S_2^{2c}(r) = r^3(1-r^2)^2,$$
$$S_2^{2s}(r) = r^5(1-r^2)^2.$$

The eigenvalues are shown in table 2. There is no sign of convergence, and it seems unlikely that the convergence will be any better at higher truncation levels.

Model 2

$$T_1(r) = 10r^4,$$
$$S_2^{2c}(r) = r^5 - r^6,$$
$$S_2^{2s}(r) = 0.07\sin^5(\pi r).$$

The eigenvalues for this model are shown in table 2. When harmonics up to degree 6 were included no plausible solution was found at all. However, the representation of the solution in the radial direction is excellent.

Model 3

$$T_1(r) = 10r^2(1-r^2),$$
$$S_2^{2c}(r) = r^2(1-r^2)^2,$$
$$S_2^{2s}(r) = 0.07\sin^5(2\pi r) \quad \text{if} \quad r < 0.5$$
$$= 0 \quad \text{if} \quad r \geqslant 0.5.$$

The eigenvalues are shown in table 2. The convergence is no better than that for Lilley's dynamo, and for two calculations no plausible solution was found at all. The eigenvector also shows irregular behaviour, but it is not included here because the convergence of the eigenvalue is so poor.

None of these models exhibit satisfactory convergence, indeed the convergence is worse than Lilley's in all three cases. Model 3 was chosen to resemble Lilley's motion, all the S_2^{2s} motion being concentrated into the inner half of the sphere, but even this shows very bad convergence.

Bullard & Gellman (1954) proposed that a meridional field could be created from their large toroidal field by a rising (or falling) and twisting motion. Although they argued that their motion did have this property, it seems unlikely in view of Braginskiĭ's results. Presumably Lilley's velocity does have this property, but it is not obvious from simply visualizing the flow. Model 4 is an attempt to put in the rising and twisting motion explicitly.

Model 4

$$\boldsymbol{u} = \boldsymbol{T}_1^0 + \boldsymbol{S}_2^{2c} + \boldsymbol{T}_3^{2c},$$

with

$$T_1(r) = 10r^4,$$

$$S_2^{2c}(r) = r^5 - r^6,$$

$$T_3^{2c}(r) = 0.07\sin^5(\pi r).$$

This model was first suggested by Bullard & Gellman (1954). It has a number of notable features. It is a simple version of the cyclonic motions envisaged by Parker (1955); it is consistent with dynamics governed by Coriolis forces, and it satisfies Braginskiĭs since-cosine criterion. In this case if Braginskiĭ's rule is not satisfied, as for example in the motion $\boldsymbol{T}_1^0 + \boldsymbol{S}_2^{2c} + \boldsymbol{T}_3^{2s}$, the 'twists' ($\boldsymbol{T}_3^{2s}$) occur midway between rising and falling currents. That such a motion would not work as an efficient dynamo is in agreement with ideas about helicity and the results from periodic dynamos. Model 4 has a positive preferred sense of helicity in the northern hemisphere, and a negative preferred sense in the southern hemisphere. The eigenvalues are shown in table 2. The convergence is no better than for any of the other models.

TABLE 2. VALUES OF THE CRITICAL MAGNETIC REYNOLDS NUMBERS FOR VARIOUS LEVELS OF TRUNCATION FOR THE FOUR MODELS STUDIED IN § 2

l is the maximum allowed degree of the harmonics and n_r is the number of radial grid points used.

	$n_r = 10$	14	16	24	30
		model 1			
$l = 2$	26.0	—	—	—	—
3	32.5	42.3	—	54.4	—
4	—	28.3	—	29.8	—
5	91.4	—	—	—	—
		model 2			
$l = 2$	15.9	—	18.3	19.1	—
3	—	—	28.0	28.1	—
4	—	—	35.2	36.9	—
5	—	—	48.4	48.9	49.2
6	—	—	None	—	—
		model 3			
$l = 3$	21.6	—	26.8	14.8	—
4	25.7	—	none	17.1	—
5	31.3	—	—	25.9	24.7
6	—	—	none	—	—
		model 4			
$l = 3$	—	—	30.9	30.0	—
4	—	—	none	none	—
5	—	—	136.5	—	—

Very few conclusions can be drawn from the failures outlined in this section. Solutions corresponding to large values of the magnetic Reynolds number are more irregular than those for small magnetic Reynolds number, which was expected. Solutions corresponding to values of R_m larger than about 200 (based on sup $|\boldsymbol{u}|$) were not adequately represented by the 30 grid points and 24 harmonics available.

Lilley's solution collapsed as more radial grid points were used, but it seemed satisfactory when more harmonics were included. This poses the problem of ensuring that the solution is receiving adequate representation in all three space variables; r, θ and ϕ. There is normally

no advantage in having a much better representation in one variable rather than any other. Series of orthogonal functions generally give a more accurate representation of smooth functions than grid points, and in this case the functions will be smooth provided R_m is not large and there are no artificial discontinuities such as Lilley's. An additional advantage of the inverse iteration method is that it is easier to be generous with grid points than with harmonics, and this has been done for all the calculations.

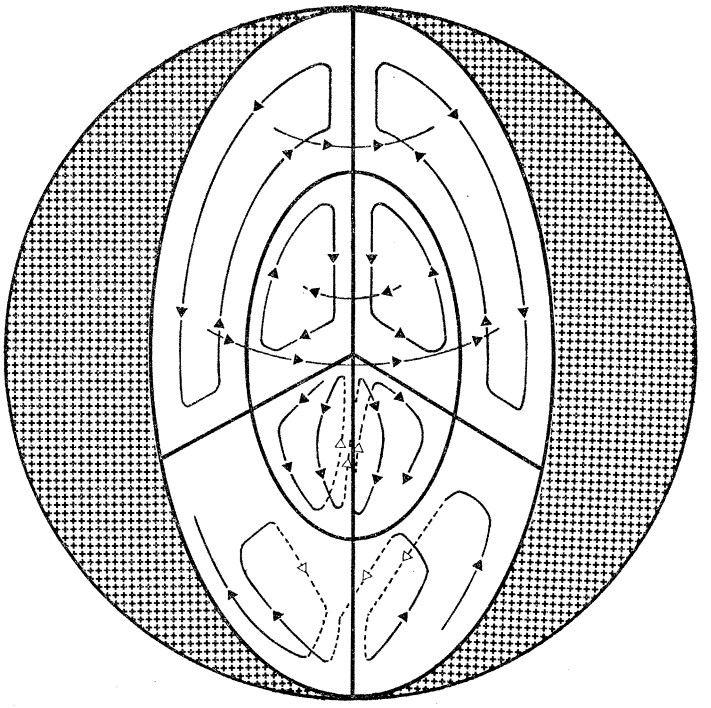

FIGURE 2. Streamlines of the flow for $n = 2$.

3. AXIALLY SYMMETRIC DYNAMOS

Now consider two scale dynamos in which the velocity, varying over a small length scale, supports a magnetic field that varies mainly over distances large compared with the length scale of the velocity. There is also an essential part of the field that is small scale, which provides the e.m.f. supporting the large scale field. Such dynamos are known to exist under certain conditions in infinite fluids, and unlike Braginskiĭ's theory the two-scale method can be applied directly to the numerical problem.

The fluid motion chosen has the form

$$\boldsymbol{u} = \epsilon \boldsymbol{S}_n + \boldsymbol{T}_n,$$

with both harmonics based on the radial function:

$$-r^2 \sin(n\pi r) \tanh n\pi(1-r). \tag{3.1}$$

When the induction equation is solved for any axially symmetric velocity, there is a set of linearly independent solutions for the field, the components of each depending on one particular $\cos m\phi$ or $\sin m\phi$ for one value of the integer m, as was pointed out in §1. The symmetry of the velocity and this simple form for the field makes the calculations considerably easier because there are fewer harmonics to be dealt with. This is a two-parameter (but not two-dimensional) problem.

The field with $m = 0$ is axisymmetric, and must decay with time because of Cowling's theorem. There is no reason to suppose, however, that fields with $m \neq 0$ cannot be supported. The solution with $m = 1$ is studied here.

Figure 2 shows the streamlines for the flow defined by equations (3.1) with $n = 2$. The streamlines are confined within any one of the cells, and are helices wrapped around the axis of symmetry. In general there are n cells radially and n between $\theta = 0$ and $\theta = \pi$. Elements of the fluid in adjacent cells move around the axis in opposite directions, but all the helices have the same right-handed sense. The motion has a preferred sense of helicity ($\overline{\boldsymbol{u}.\operatorname{curl}\boldsymbol{u}}$, where the overbar denotes an average over many cells) throughout the sphere. This is in contrast to Roberts's motion (Zmuda 1971) which has helicity with opposite signs in the upper and lower hemispheres. Otherwise the two motions are very similar; this one fits into a sphere more satisfactorily, and the differences could hardly be expected to influence the dynamo action drastically.

A two-scale analysis of the problem is possible when n is large. Childress (1970) has shown that provided the length scale of the motion is sufficiently small compared with the dimensions of the sphere, then the boundaries have no significant effect on the small-scale fields. We may therefore ignore the effects of the boundaries except in solving for the large-scale field. An averaging procedure must be defined for any two-scale approximation, and the one appropriate here is over an angle θ_0, and a radial distance r_0, which define an area large compared with the size of one of the cells, but small in relation to the whole sphere.

The procedure now is to solve equation (1.6) for the small scale field $\boldsymbol{B}'$ in terms of $\boldsymbol{u}$ and $\boldsymbol{B}_0$ by some method such as Fourier transforming, and substitute back into equation (1.5) to solve for $\boldsymbol{B}_0$. Following, for example, Moffatt (1970), the e.m.f. $\overline{\boldsymbol{u}\times\boldsymbol{B}'}$ may be written in the form:

$$\overline{(\boldsymbol{u}\times\boldsymbol{B}')}_i = A_{ij}B_{0j}, \tag{3.2}$$

where the tensor $\boldsymbol{A}$ is related to $\boldsymbol{u}$ and the resistivity. For any homogeneous motion, such as homogeneous turbulence or periodic motions, the tensor $\boldsymbol{A}$ is independent of position, provided the right averaging procedure is used. For homogeneous isotropic turbulence $\boldsymbol{A}$ reduces to the form $\alpha\delta_{ij}$, but this is not the case for periodic motions in general because they are not isotropic. As an example consider the motion

$$\boldsymbol{u} = U(x,y)\,\boldsymbol{e}_z + \epsilon\operatorname{curl}[U(x,y)\,\boldsymbol{e}_z], \tag{3.3}$$

where

$$U(x,y) = u_0\cos(kx+ky)\cos(kx-ky).$$

This gives the tensor (G. O. Roberts 1970):

$$\boldsymbol{A} = \alpha\begin{pmatrix}1&0&0\\0&1&0\\0&0&0\end{pmatrix}, \tag{3.4}$$

where the overbar denotes an average over one wavelength. In this case $\boldsymbol{B}_0$ has no z-component, and this form for $\boldsymbol{A}$ can be replaced by $\alpha\delta_{ij}$ for the purpose of calculating the mean e.m.f. (3.2). However, the choice

$$U(x,y) = u_0\cos(k_x x+k_y y)\cos(k_x x-k_y y),$$

with $k_x \neq k_y$ does not give a diagonal tensor.

It is possible to apply a similar analysis to the spherical harmonic motion, but a simple form for $\overline{\boldsymbol{u}\times\boldsymbol{B}'}$ does not emerge. However, the analysis can be used in effecting approximate numerical solutions, and this is discussed later in this section. Also it is still reasonable to suppose that the dynamo mechanism acting is one in which a current is produced parallel to the mean field $\boldsymbol{B}_0$.

PHILOSOPHICAL TRANSACTIONS OF THE ROYAL SOCIETY A MATHEMATICAL, PHYSICAL & ENGINEERING SCIENCES

With the $m = 1$ solution, the first degree harmonics are S_1^1 and T_1^1, an equatorial dipole and a toroidal field symmetric about the same axis. If an 'α-effect' is operating, T_1^1 will be produced from S_1^1 and vice versa. One may therefore expect the field to consist predominantly of these two harmonics, with a smaller field varying on the same length scale as the velocity.

These theoretical considerations are useful in finding the rough form of the expected solution, but they only apply in the limit $n \to \infty$, and therefore n must be chosen as large as possible. On the other hand, for a numerical solution it is essential to represent the velocity and the small scale field adequately. The available computing facilities made 6 the largest value of n that could be dealt with.

Three dynamo models have been chosen to study the convergence of the scheme, with $n = 6$, 4 and 2. ϵ was taken as $\frac{1}{30}$ for $n = 6$ and $n = 4$, and $\frac{1}{10}$ for $n = 2$; the importance of this parameter will be discussed later.

The solution for $R_m = 0$ was compared with the analytical value. Three significant figure accuracy was obtained for the decay rate $-\pi^2$ by the use of 100 grid points.

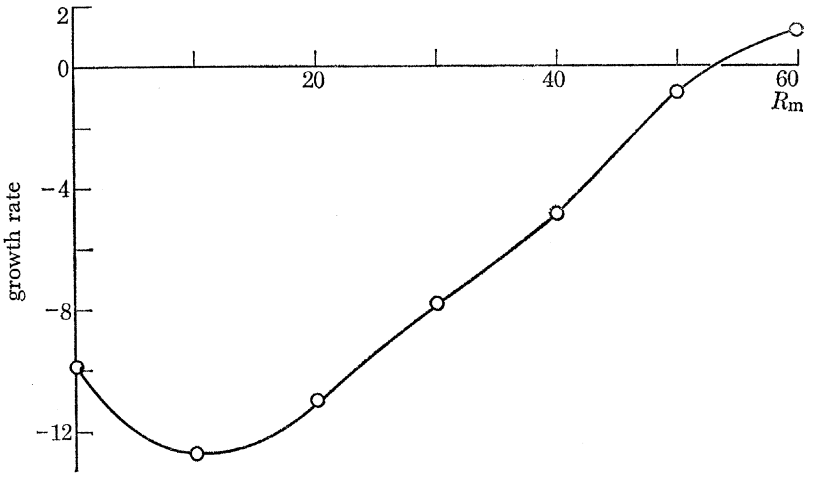

FIGURE 3. Growth rate: $\sigma = \mathrm{Re}\,(p)$ as a function of magnetic Reynolds number for the model with $n = 2$, $\epsilon = \frac{1}{30}$.

TABLE 3. EIGENVALUES σ FOR THE MODEL WITH $n = 2$, $\epsilon = \frac{1}{10}$ FOR $R_m = 60$

The value in brackets was found by the use of double precision.

	$n_r = 25$	51	75	99
$l = 6$	1.10	1.31	—	—
7	2.61	2.70	—	—
8	2.49	2.60 (2.61)	—	—
9	1.86	2.01	—	—
10	1.97	2.11	—	—
11	2.11	2.24	—	—
12	2.10	2.22	2.26	2.26
13	2.04	—	—	—
14	2.06	—	—	—
15	2.06	—	—	—

Solutions for $n = 2$, $\epsilon = \frac{1}{10}$

Solutions were found for magnetic Reynolds numbers of 10, 20, 30, 40, 50 and 60. In all cases the eigenvalue $p = \sigma + i\omega$ was real, indicating that the field simply grows or decays with time, with

no oscillation or rotation. The growth rate σ is plotted against R_m in figure 3; these results were obtained using 25 grid points and harmonics up to degree 6. There is a steady state near $R_m = 53$. The field for this value of R_m at the same level of approximation is shown in figure 4. The radial variation seems to be well represented by 25 grid points, and the harmonics of degree 6 are quite small.

The numerical convergence of these solutions requires a rigorous check because so many disasters have occurred already. There are three sources of errors: an insufficient number of harmonics, an insufficient number of grid points, and rounding errors. Each of these has been checked, either by taking more harmonics, more grid points, or repeating some of the calculations in double precision. The results at $R_m = 60$ are summarized in table 3. This eigenvalue has converged to two decimal places, but this is not the significant criterion for convergence. The growth rate for the largest magnetic Reynolds number will be the most inaccurate of all the points on the curve of $\sigma(R_m)$ in figure 3. This view is confirmed by examining the convergence of the values for $R_m = 40$ and $R_m = 50$ in table 4. Therefore the error in the growth rate for $R_m = 60$ defines limits for the true position of the whole curve shown in figure 3. The error in the growth rate should therefore be compared with π^2 to give a true estimate of the convergence. Alternatively, if one expresses the convergence in terms of the magnetic Reynolds number for a steady state (as Lilley (1970) does), the result will depend on the gradient of the curve as it crosses the axis. Here it appears to have converged to about 0.02 %, which is much better than previous estimates of convergence of this number. It is possible to extrapolate from the table of eigenvalues to find a more accurate estimate of the growth rate, but this provides no more information about either the convergence, or the mechanism of the dynamo.

TABLE 4. TESTS OF CONVERGENCE FOR $n = 2$, $\epsilon = \frac{1}{10}$

l	n_r	σ
	$R_m = 40$	
6	25	−4.86
8	51	−4.17
	$R_m = 50$	
6	25	−1.85
8	51	−0.78
10	51	−1.06

Figure 4 also contains the field for $R_m = 60$ at the higher level of approximation $l = 10$, $n_r = 51$. These eigenvectors have been normalized so that the sum of the absolute values of the first 12 harmonics is proportional to the number of grid points used, making the total area under the first twelve curves the same in both cases. The agreement between these two sets of curves is very good considering that the difference between the two levels of approximation is almost a factor of 2 both in the number of grid points and the number of harmonics. The first-degree harmonics S_1^1 and T_1^1 are the largest ones. This was expected, although the $n = 2$ motion is by no means small scale. The magnitudes of the harmonics of degrees 9 and 10 are about 1 % of the first degree ones.

The one calculation carried out in double precision was the largest that could be done with the computing facilities available. The agreement with the single precision calculation is very good,

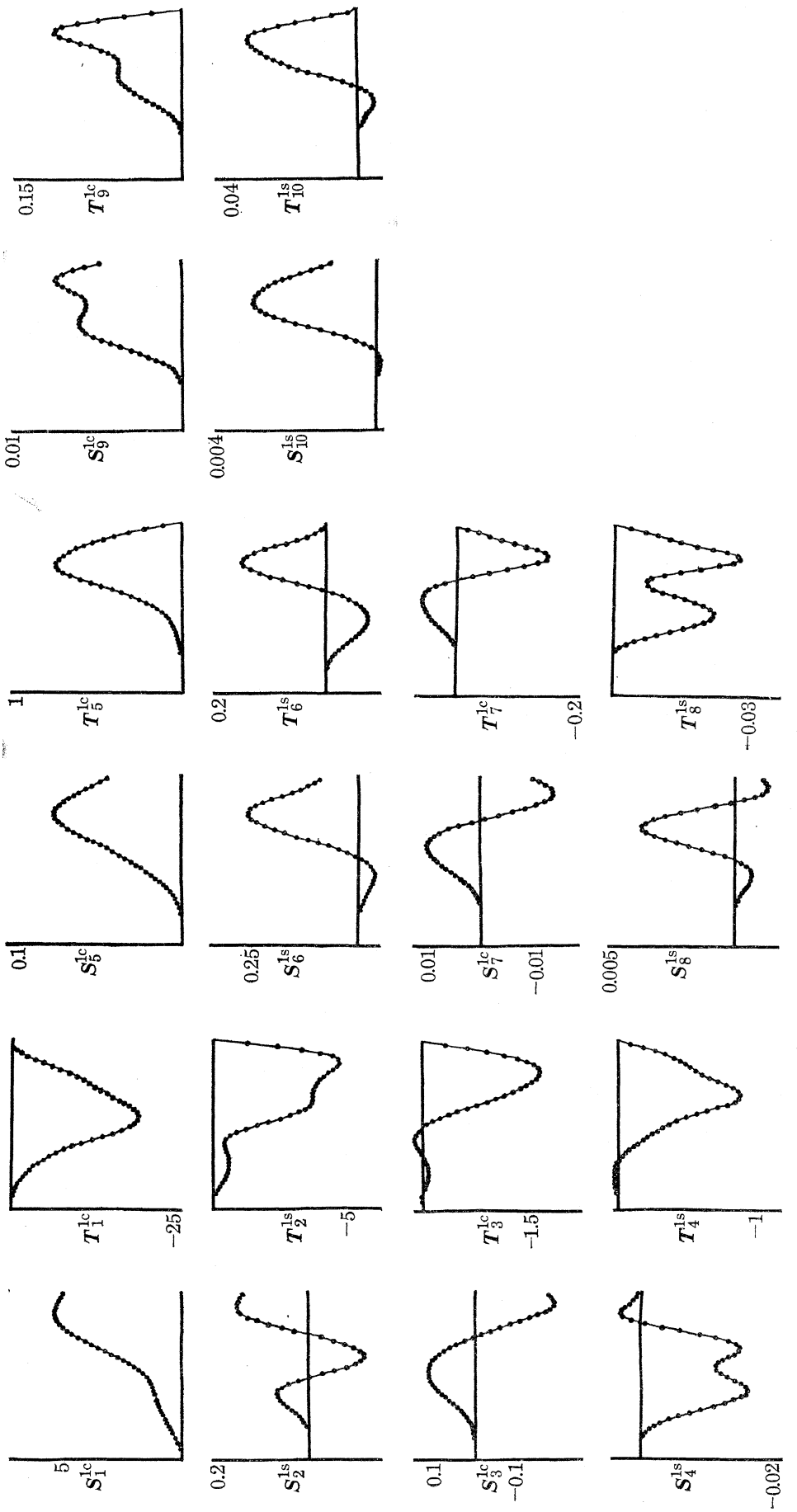

FIGURE 4. Magnetic field solutions for the case $n = 2$, $\epsilon = \frac{1}{10}$ at two levels of approximation: $l = 6$, $n_t = 25$ for the upper solution; $l = 10$, $n_t = 51$ for the lower solution.

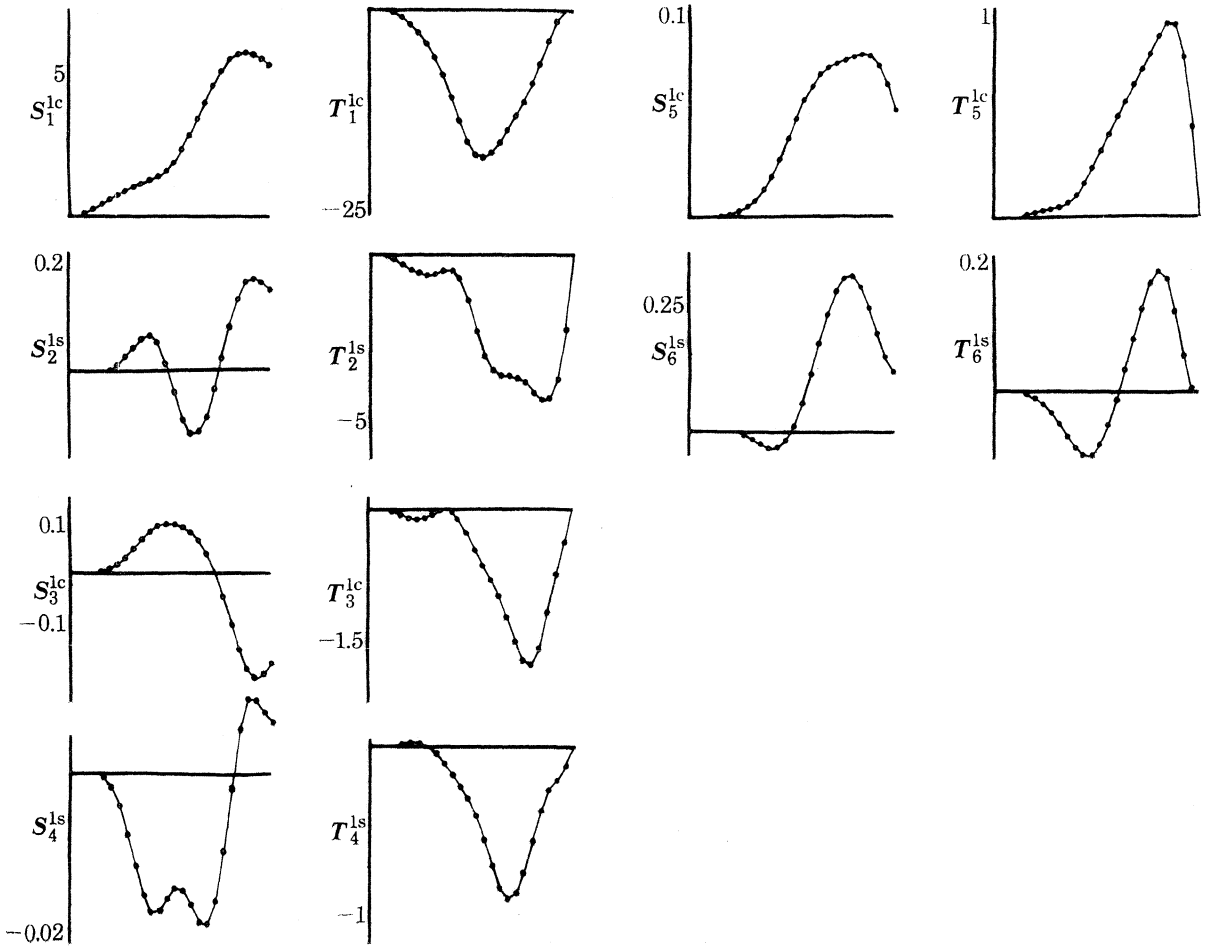

PHILOSOPHICAL TRANSACTIONS OF THE ROYAL SOCIETY A MATHEMATICAL, PHYSICAL & ENGINEERING SCIENCES

which suggests that all the single precision values up to that level of approximation will be satisfactory. The higher calculations will be more susceptible to rounding errors and could not be checked, but they show no signs of accumulating errors.

It is difficult to establish whether the eigenvalues have a small or a zero imaginary part. The method used to check for convergence of the inverse iteration scheme was to subtract successive approximations to the eigenvector and average the moduli of the resulting components. This number was required to be less than a certain test value. In single precision the computer kept 7 significant figures, so that in taking the modulus the imaginary part of the eigenvector has no significance if it is less than 10^{-4} of the real part. In double precision 16 significant figures are kept, and an imaginary part less than 10^{-8} times the real part has no significance. For both the single and double precision calculations carried out, the imaginary parts of the eigenvectors had no significance. The eigenvalues are deduced to be real, and in §4 arguments are put forward to show that this should always be the case when n is even.

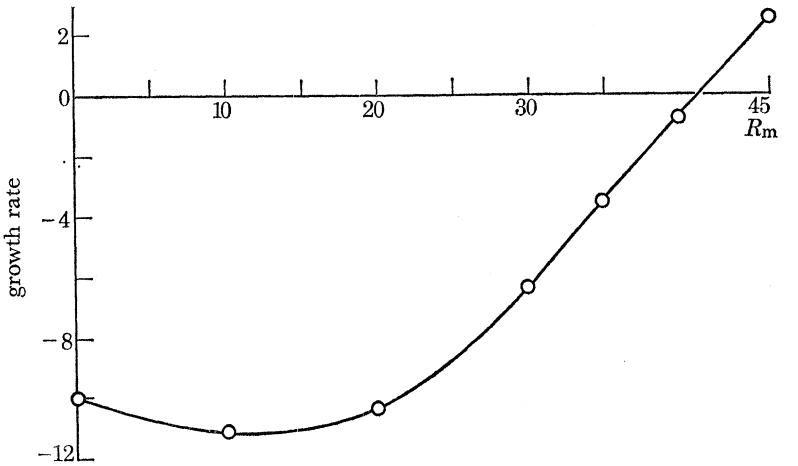

FIGURE 5. Growth rate as a function of magnetic Reynolds number for the model with $n = 4$, $\epsilon = \frac{1}{30}$.

TABLE 5. TESTS OF CONVERGENCE WITH $n = 4$, $\epsilon = \frac{1}{30}$, $R_m = 40$

	$n_r = 25$	51
$l = 6$	−0.72	—
8	—	−0.90
		(−0.90)
10	—	−3.41
12	—	−3.44

Solutions for $n = 4$, $\epsilon = \frac{1}{30}$

The eigenvalues for this model are plotted against R_m in figure 5 for the approximation $l = 6$, $n_r = 25$. There is a steady solution near $R_m = 40$. The convergence of this solution was studied; the results are in table 5. The field for the approximation with $l = 12$, $n_r = 51$ and $R_m = 40$ is shown in figure 6. It is comprised mainly of the two first degree harmonics S_1^1 and T_1^1. Also notice that the 'small-scale' field, that is the one on the same scale as the velocity with harmonics of degrees 3, 4 and 5, is small scale in the radial direction as well as with θ_0.

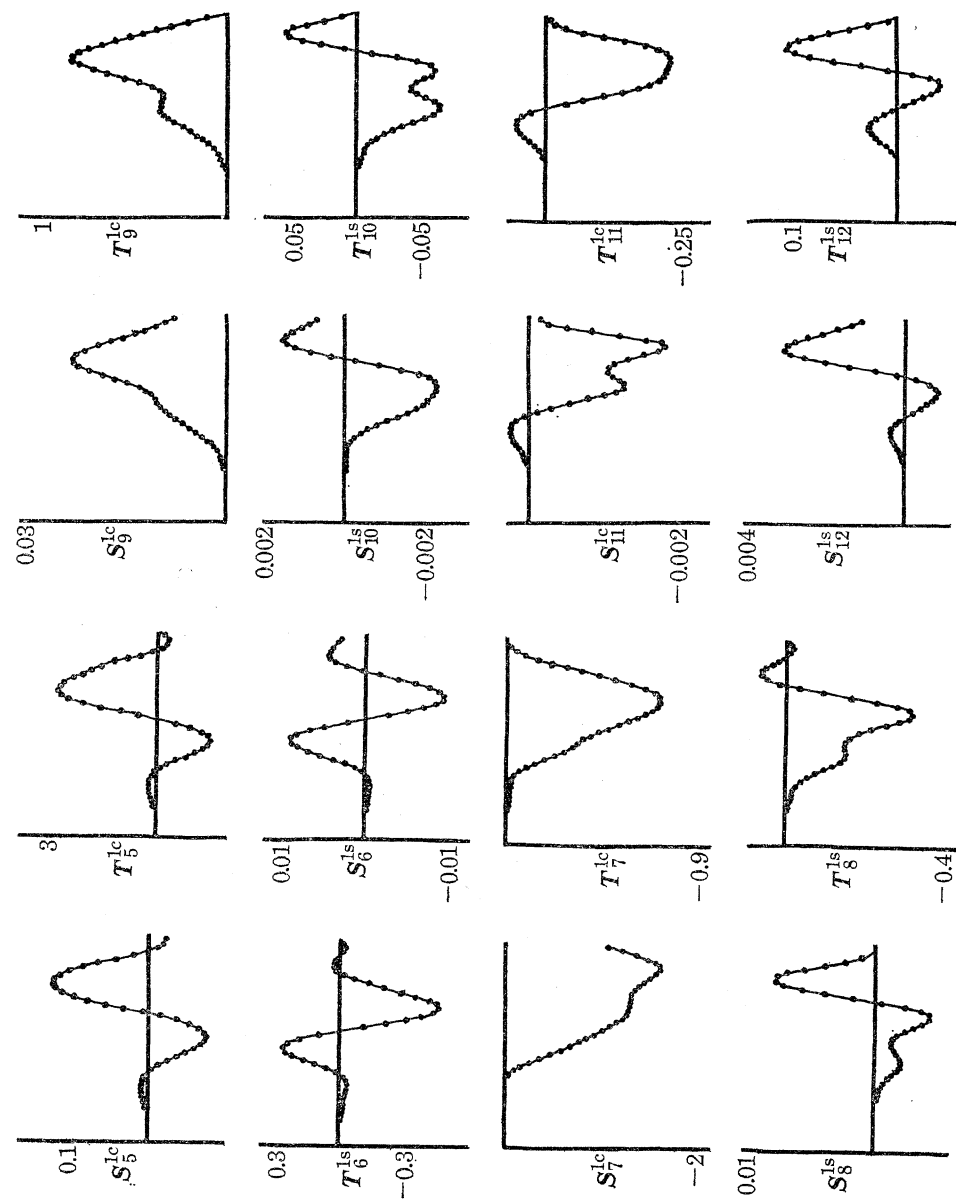

FIGURE 6. Magnetic field solutions for the case $n = 4$, $\epsilon = \frac{1}{30}$, for the approximation $l = 12$, $n_r = 51$.

Solutions for $n = 6$, $\epsilon = \frac{1}{30}$

Growth rates and the corresponding fields were calculated using harmonics up to degree 8 and 51 grid points. The plot of growth rate against R_m is shown in figure 7. The field is steady near $R_m = 30$, and this solution was tested for convergence. The results are shown in table 6. The rounding errors are more severe, although the double precision calculation should be accurate. Fifty-one grid points seem adequate, but the convergence as the number of harmonics is increased is poor.

TABLE 6. TESTS OF CONVERGENCE FOR $n = 6$, $\epsilon = \frac{1}{30}$, $R_m = 30$

	$n_r = 51$	99
$l = 8$	1.20	1.27
	(1.09)	
10	3.14	—
12	—	−0.71

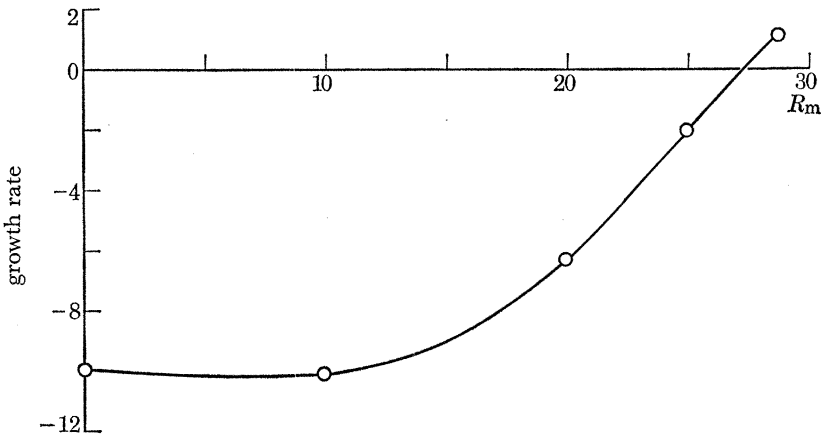

FIGURE 7. Growth rate as a function of magnetic Reynolds number for the case $n = 6$, $\epsilon = \frac{1}{30}$.

The field for the $l = 12$, $n_r = 99$ and the $l = 8$, $n_r = 51$ approximations are shown in figure 8. The agreement between the two approximations is not very good. The degree 2 harmonics are as large as those of degree 1, which may be why the convergence in this case is not as good as the others. It also shows that a full examination of the field is much more revealing than merely looking at the eigenvalues.

Solutions for a modified velocity with $n = 6$ and $\epsilon = \frac{1}{30}$

Some calculations were carried out with a velocity which has the form (3.1) but with radial function.

$$-r \sin n\pi r \tanh n\pi(1-r). \tag{3.5}$$

This velocity has a discontinuity in the meridional components at $r = 0$, but in spite of this there is no problem in solving the equations. The solutions are similar to those for the previous motion, but one calculation is included here because of the improved convergence that can be obtained for $n = 6$. The extra power of r in velocity (3.1) has the effect of making the field a more rapidly varying function of position near the boundary of the sphere, so that numerical representation is more difficult there.

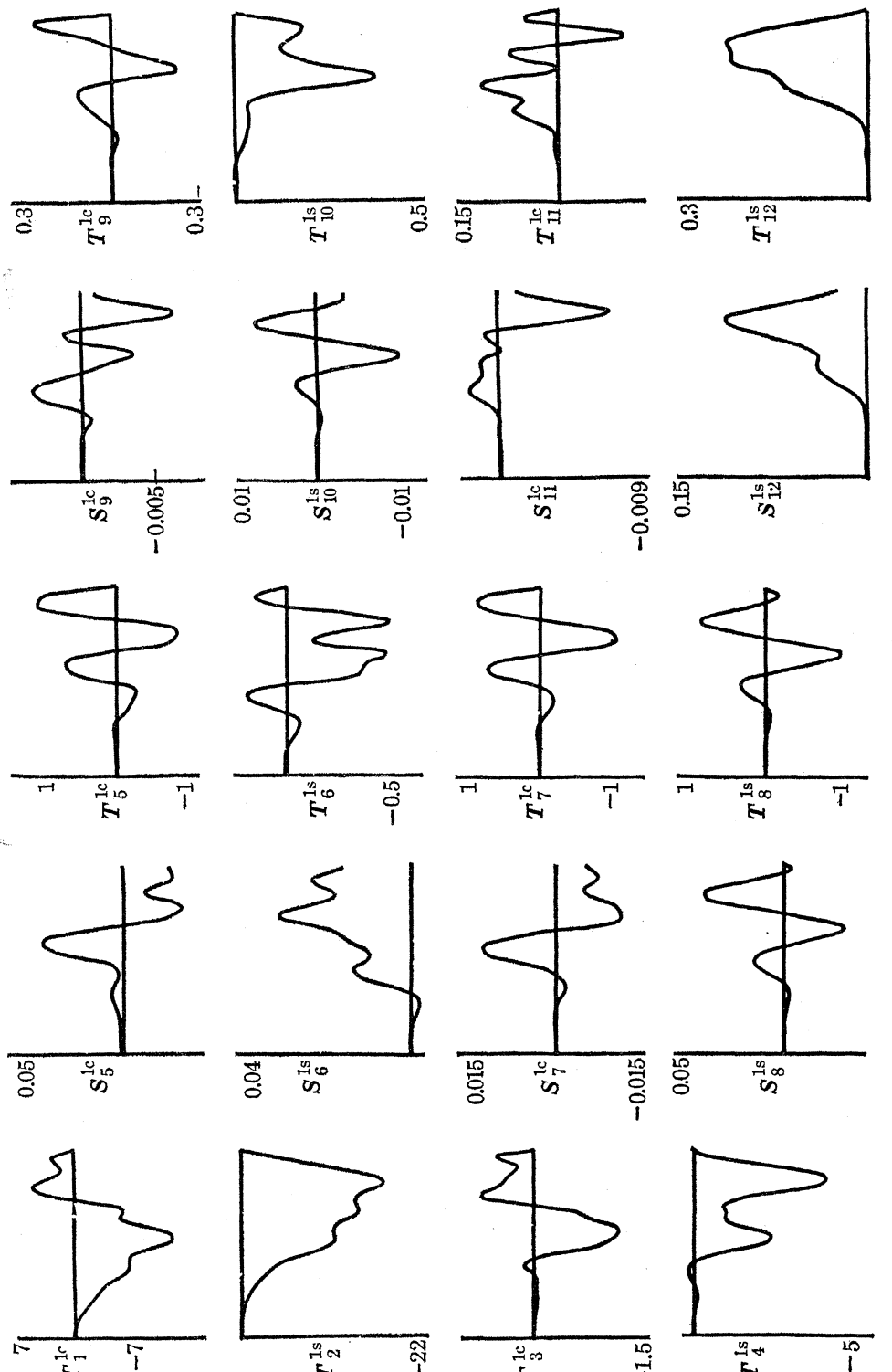

FIGURE 8. Magnetic field solutions for the case $n = 6$, $\epsilon = \frac{1}{30}$, for velocity (3.5) and the approximation $l = 12$, $n_t = 99$.

PHILOSOPHICAL TRANSACTIONS OF THE ROYAL SOCIETY A MATHEMATICAL, PHYSICAL & ENGINEERING SCIENCES

The value of ϵ chosen for the model was $\frac{1}{30}$. The steady state is near $R_m = 16$. This is about half the corresponding value for the original velocity, which is reasonable because the extra power of r in (3.1) will reduce the typical scale of the velocity by half. The solution at $R_m = 16$ converges well, as is shown in table 7. The first degree harmonics for the field are the dominant ones, all the others are very much smaller in size. The radial functions all behave well at the origin; a close examination shows that those for the two first-degree harmonics satisfy the requirements:

$$S_1^{1c}(r) = 0(r^2), \quad T_1^{1c}(r) = O(r^3).$$

TABLE 7. TESTS OF CONVERGENCE FOR THE MODIFIED VELOCITY, WITH $n = 6$, $\epsilon = \frac{1}{30}$ AND $R_m = 16$

	$n_r = 51$	99
$l = 8$	1.25	1.40
9	1.97	—
	(1.96)	
10	1.97	—
12	—	2.05

This concludes the demonstrations of convergence. It is convincing not only because the answers are well behaved, but also because they fit with what one would expect on theoretical grounds. With the possible exception of the third model, these results are incomparably better than any of those in § 2.

It is possible to solve the two simplified equations (1.5) and (1.6) for both the small- and large-scale fields by a spherical harmonic expansion similar to the Bullard–Gellman technique for the induction equation. It is reasonable to suppose that the large-scale field can be represented accurately by a sum of harmonics with degrees 1 to s, where $s \ll n$. n appears in the velocity (3.1) and defines the small-length scale. The small-scale field can be represented by a sum of harmonics with degrees near n. Consider equation (1.6). Small-scale field $\boldsymbol{B}'$ is produced directly from the interaction between $\boldsymbol{u}$ and $\boldsymbol{B}_0$, the interaction between $\boldsymbol{u}$ and the small-scale field being neglected. There are selection rules (Bullard & Gellman 1954, rules 1 (b) and 2 (b)) which only allow interactions between harmonics with degrees that can form the sides of a triangle, and so $\boldsymbol{B}'$ in equation (1.6) will only contain harmonics with degrees $n-s$ to $n+s$.

This proposed solution of the equations (1.5) and (1.6) is exactly equivalent to a Bullard–Gellman solution of the induction equation in which certain interactions are neglected. First, all field harmonics with degrees other than 1 to s or $n-s$ to $n+s$ are neglected. Of all the interactions between these harmonics, the only ones to be retained are those that produce harmonics of one band from harmonics of the other, that is through the terms $\boldsymbol{u} \times \boldsymbol{B}_0$ or $\overline{\boldsymbol{u} \times \boldsymbol{B}'}$. Other interactions, such as the production of large degree harmonics from other large degree harmonics (the term $\boldsymbol{u} \times \boldsymbol{B}' - \overline{\boldsymbol{u} \times \boldsymbol{B}'}$) are neglected.

Taking $n = 6$ and only first degree harmonics for $\boldsymbol{B}_0$ ($s = 1$), there is a simple interaction diagram, shown in figure 9. The arrows denote whether small- or large-scale field is being produced, and the velocity harmonic is written next to it. When the second- and third-degree harmonics are included in the series for $\boldsymbol{B}_0$, the two-scale approximation breaks down altogether because both $\boldsymbol{B}_0$ and $\boldsymbol{B}'$ have third-degree harmonics; their length scales overlap. It is clear now that when the full induction equation is solved for this problem with $n = 6$, up to degree 8 for example, it only accounts for the maintenance of the first- and second-degree harmonics of $\boldsymbol{B}_0$ plus some, but not all, of the interactions maintaining the third degree harmonics.

PHILOSOPHICAL TRANSACTIONS OF THE ROYAL SOCIETY A MATHEMATICAL, PHYSICAL & ENGINEERING SCIENCES

This approximate method of solution has been applied to the second velocity (3.5) with $n = 6$ and $\epsilon = \frac{1}{30}$. An examination of the field for this solution suggests that $\boldsymbol{B}_0$ might be represented by the first degree harmonics alone, and therefore harmonics of degrees 5 to 7 are adequate for the small-scale fields. Fifty grid points were used to solve the equations. The eigenvalues are shown in figure 10, where they may be compared with the full solutions reported earlier. The agreement is generally very good, and as would be expected the differences increase as R_m increases.

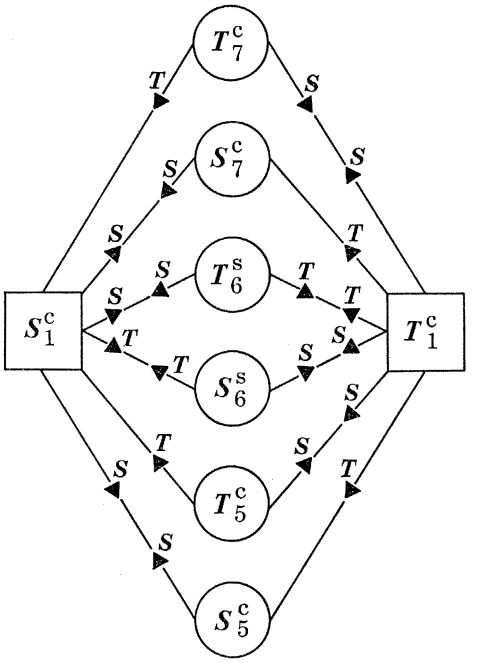

FIGURE 9. Interactions between the first degree harmonics and the small scale field for the S_6, T_6 dynamo.

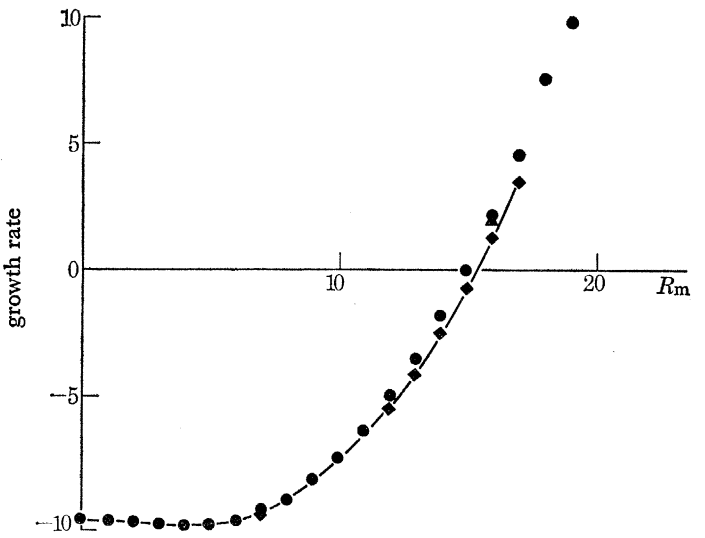

FIGURE 10. Growth rate as a function of magnetic Reynolds number for the case $n = 6$, $\epsilon = \frac{1}{30}$ and velocity (3.5) for three different approximations: ●, by the approximate method with $s = 1$ (see text); ◆, $l = 8$, $n_r = 51$; ▲, $l = 12$, $n_r = 99$.

This approximate method of solution corroborates the view that these dynamos do work on a two-scale mechanism. The solution with $n = 6$ appears to be accurate, and one would expect this accuracy to improve as n increases. It therefore offers a quick way of investigating dynamos with large n, which would not be possible by solving the full problem. It has been used successfully on dynamos with $n = 8$, 10 and 12.

4. Physical properties of the axially symmetric dynamos

Having solved the difficult problem of the convergence of the numerical methods, the physical properties of these dynamos may be investigated more fully. Both types of velocity studied depend on the parameters n and ϵ. The product $n\epsilon$ is the estimate of the ratio of poloidal motion to toroidal motion.

A suitable definition is needed for the magnetic Reynolds number $R_m = \mathscr{L}\mathscr{U}/\lambda$, and there is a problem in the choice of the scale of the velocity. Two scales are available that are not trivially related to each other. One possibility is to choose: $\mathscr{U} = \sup |\boldsymbol{u}|$. Alternatively, we may take $\mathscr{U} = 1$. Problems arise because the maximum values of the Legendre functions depend on n:

$n =$	2	4	6	8	10	12
$[P_n^1(\cos\theta)]_{\max}$	1.50	2.64	3.80	4.96	6.12	7.28

Therefore magnetic Reynolds numbers of dynamos with different values of n are compared, the result will depend on the definition used for R_m. The latter definition seems the best and is the one used here.

Initially the calculations were restricted to even n, which always have real time constants for the field, and for which steady solutions exist for some value of R_m. Once the eigenvalues are known to be real it is possible to save a factor of two in computer storage. A useful parameter is the critical magnetic Reynolds number, R_m^c, which is the value of R_m for which the field is steady. It is a function of n and ϵ, and is a gauge of the efficiency of the dynamo.

The dependence of R_m^c on n and ϵ can be studied numerically, and may also be estimated from the two-scale approximation. First consider the validity of equations (1.5) and (1.6) in view of the results already obtained in § 3. The essential requirements are that

$$|\boldsymbol{B}'| \ll |\boldsymbol{B}_0|, \quad |\nabla \boldsymbol{B}'| \simeq |\nabla \boldsymbol{B}_0|,$$

and the fields calculated in § 3 do seem to have this property. However, the assumptions made are adequate provided that the magnetic Reynolds number based on the small length scale, that is R_m/n, is small. This is not true for the solutions of § 3, where

$$R_m/n \gtrsim 1.$$

This quantity would appear to be too large for the two-scale method to work; n needs to be at least an order of magnitude larger to make R_m/n small. This important point is discussed later.

Taking the radius of the sphere to be unity and following either Childress (1967) or Moffatt (1970), we may deduce an order of magnitude estimate for $\boldsymbol{B}'$:

$$|\boldsymbol{B}'| \simeq \frac{1}{\lambda n^2} \overline{\boldsymbol{u} . \operatorname{curl} \boldsymbol{u}}\, |\boldsymbol{B}_0|. \tag{4.1}$$

A similar result applies for isotropic turbulence, and also it can be assumed to hold for the motions in (3.1) and (3.5) provided n is large enough. For these motions

$$\overline{\boldsymbol{u}.\operatorname{curl}\boldsymbol{u}} \sim n^2\epsilon u_0^2,$$

where u_0 is the typical toroidal velocity. For a steady solution, equation (1.5) gives:

$$\frac{u_0^2\epsilon}{\lambda}|\boldsymbol{B}_0| \simeq \lambda|\boldsymbol{B}_0|$$

and therefore

$$R_{\mathrm{m}}^{\mathrm{c}} = \frac{u_0}{\lambda} \simeq \frac{1}{\epsilon^{\frac{1}{2}}}. \tag{4.2}$$

The critical magnetic Reynolds number should be independent of n for this choice of motion.

Values of the critical magnetic Reynolds number for velocity (3.5) at three values of ϵ are shown in table 8, and for velocity (3.1) at two values of ϵ in table 9. $R_{\mathrm{m}}^{\mathrm{c}}$ was estimated very approximately from the curve of growth rate against R_{m}. These tables demonstrate the most important and interesting properties of the dynamos. $R_{\mathrm{m}}^{\mathrm{c}}$ is roughly constant, although it is larger for smaller numbers of cells. This may be due to the definition of R_{m}, or it may be an effect due to the boundaries. As n increases, $R_{\mathrm{m}}^{\mathrm{c}}$ appears to settle down to a finite limit rather than to zero or infinity.

For motion (3.5) there are only growing solutions for a band of values of n at any fixed value of ϵ. Table 8 suggests that, for this motion at least, fields can only be supported for a certain range of the parameter $n\epsilon$. For those solutions that do have growing fields, the dependence of $R_{\mathrm{m}}^{\mathrm{c}}$ on ϵ agrees qualitatively with the expected $\epsilon^{-\frac{1}{2}}$ variation.

TABLE 8. VARIATION OF $R_{\mathrm{m}}^{\mathrm{c}}$ WITH n AND ϵ FOR VELOCITY (3.5)

	$n=2$	4	6	8	10	12
$\epsilon = \frac{1}{10}$	33	16	12	12.5	no positive solution found	
$\frac{1}{30}$	no positive solution found		15	13	11.5	12
$\frac{1}{60}$	no positive solution found		26	18	16	16

TABLE 9. VARIATION OF $R_{\mathrm{m}}^{\mathrm{c}}$ WITH n AND ϵ FOR VELOCITY (3.1).
NUMBERS IN BRACKETS ARE UNCERTAIN

	$n=2$	3	4	6	8	10	12
$\epsilon = \frac{1}{10}$	60	30	—	20	solutions unreliable		
$\frac{1}{30}$	no positive growth found		40	30	(21)	(22)	(23)

A motion with one radial cell and two angular (θ) cells was investigated and does not appear to work at any magnetic Reynolds number. The motion is given by

$$\boldsymbol{u} = \epsilon\boldsymbol{S}_2 + \boldsymbol{T}_2$$

with radial function $-r^2\sin\pi r\tanh n\pi(1-r)$. There was no positive growth rate for $\epsilon = \frac{1}{10}$ or $\epsilon = \frac{1}{20}$.

Occasionally secondary solutions have been found that have a smaller growth rate than the one of primary interest. This suggests that there are other modes which decay more rapidly

than the principal one, perhaps corresponding to a different decay mode of a solid sphere. These modes certainly exist for α-effect dynamos, but they have not been studied in detail in these numerical models.

The cutoff function $\tanh n\pi(1-r)$ was removed for some of the calculations. The resulting fields had sharp gradients near the boundaries, and the convergence of the solutions was poor, showing that it is desirable to have zero gradient in the angular velocity at the boundary. A finite shear at the boundary produces a toroidal field there, which creates numerical problems when the boundary conditions are applied.

When the parameter $n\epsilon$ exceeds a certain critical value the solutions take on a rope-like structure. This is because the poloidal motion in any one of the cells is strong enough to expel the magnetic flux into narrow regions at the cell boundaries. This expulsion of flux by eddies has been studied by Weiss (1966) and R. L. Parker (1966).

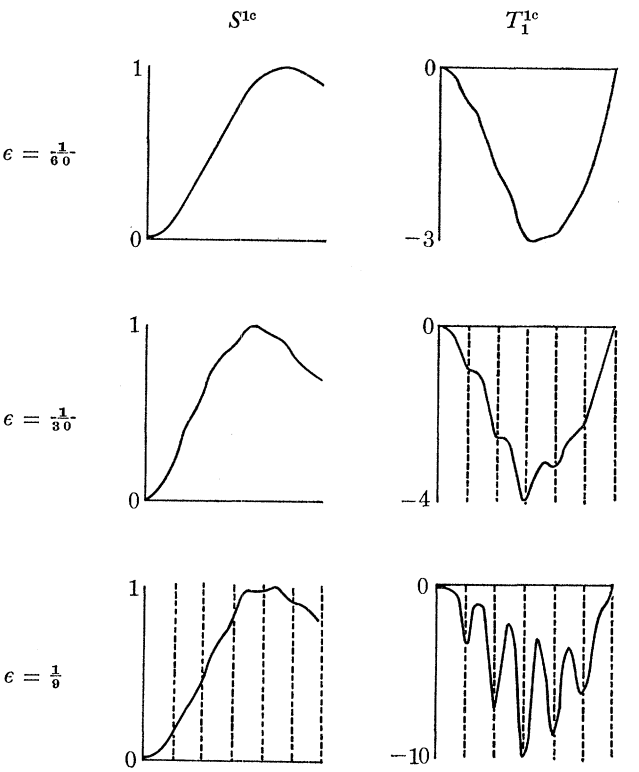

FIGURE 11. Radial functions for the S_1^1 and T_1^1 harmonics for velocity (3.5), $n = 6$ and three values of ϵ. The expulsion of toroidal flux may be seen as ϵ is increased.

Consider, for example, the solution for velocity (3.5), $n = 6$ and $\epsilon = \frac{1}{30}$. For small ϵ the field is comprised mainly of the first-degree harmonics. Of these the toroidal field is directed, for the most part, across the eddies and will be expelled by them if the motion is vigorous enough. On the other hand, the poloidal field is largely parallel to the eddies and will be little affected by them.

Figure 11 illustrates this expulsion of flux. The main poloidal and toroidal fields are compared for $n = 6_0$ $R_m = 16$ and three values of ϵ. At this magnetic Reynolds number, the lower two

fields belong to growing solutions but the upper one is decaying. The cell boundaries are marked with dotted lines. Clearly the toroidal flux is being expelled into narrow regions which are exactly on the cell boundaries. The dipole field is only slightly affected.

The field must also be forced into cones of constant θ, which are cell boundaries as well as the spherical shells of constant r marked by dotted lines in figure 1. The numerical representation of such a field requires a large number of grid points and harmonics. This presents considerable numerical problems, and the results are inconclusive. There may be sufficient grid points for the sample calculation in figure 11, but certainly degree 12 in the harmonics is not enough when the flow contains harmonics of degree 6.

It is possible to obtain reasonably convergent solutions with large values of ϵ when $n = 2$, but because there are only four cells in this motion it is not really typical of small scale dynamos. Results have been obtained for both velocities:

		l	n_r	σ
velocity (3.1)	$n = 2, \epsilon = \frac{1}{3}; R_m = 30$	6	25	1.83
		8	51	3.76
velocity (3.5)	$n = 2, \epsilon = \frac{1}{5}; R_m = 20$	6	25	−19.71
		8	51	−16.70
		10	51	−17.19

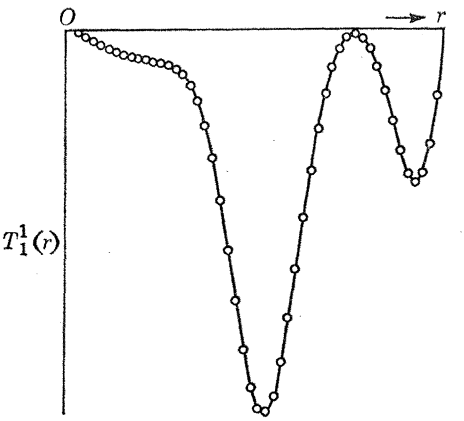

FIGURE 12. Radial function for the T_1^1 harmonic for velocity (3.1), $n = 2$, $\epsilon = \frac{1}{3}$.

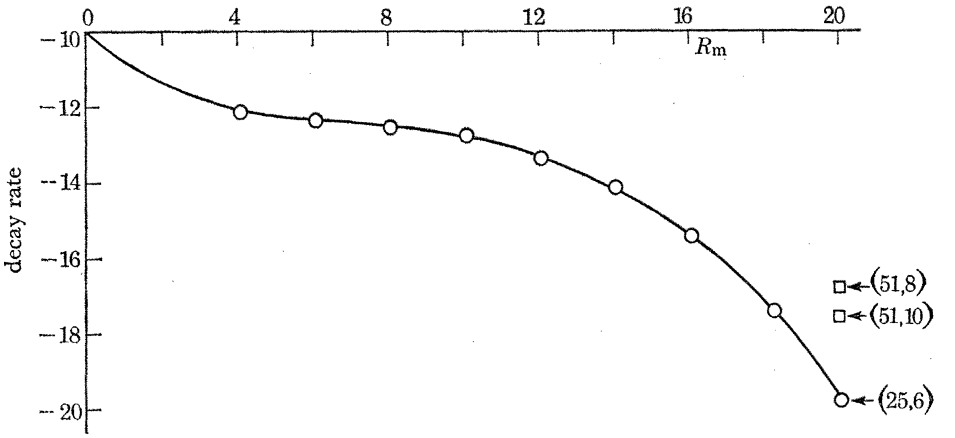

FIGURE 13. Growth rate as a function of magnetic Reynolds number for velocity (3.1), $n = 2$, $\epsilon = \frac{1}{3}$. Values in parentheses give n_r and l.

Figure 12 shows the radial function of the toroidal field for the first case. The flux is concentrated near $r = 0.5$, the cell boundaries. Numerical difficulties have prevented establishing whether or not velocity (3.5) can support fields when ϵ is large. The plot of $\sigma(R_m)$ for this flow when $n = 2$, $\epsilon = \frac{1}{3}$ is shown in figure 13, together with the values used to check the convergence. There is no sign that the growth rate becomes positive, or even exceeds the value $-\pi^2$ that characterises a sphere with no motion.

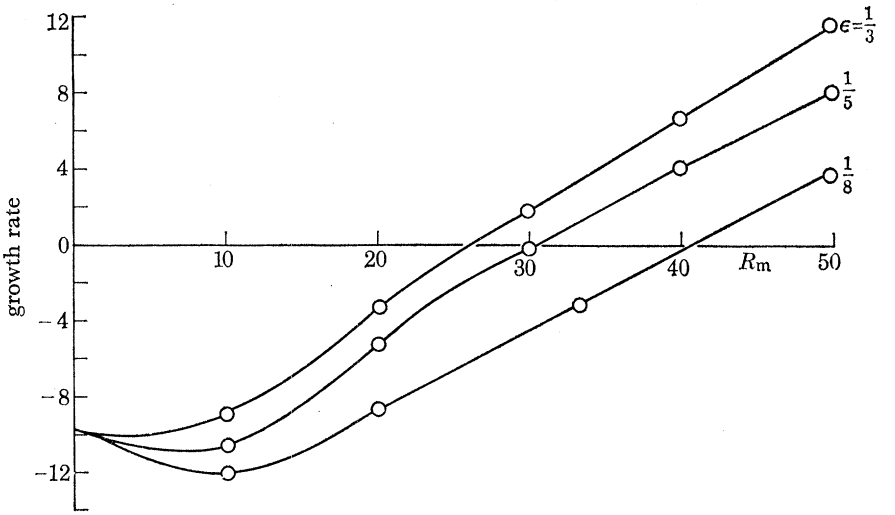

FIGURE 14. Growth rate as a function of magnetic Reynolds number for velocity (3.1), $n = 2$ and three values of ϵ.

The results for velocity (3.1) are completely different. Figure 14 shows the graphs of $\sigma(R_m)$ for $n = 2$ and three values of ϵ. There is a shape to each curve which is typical of all the solutions found. For small R_m the growth rate falls below $-\pi^2$, then it rises. All of these dynamos seem to work satisfactorily, and calculations done on dynamos with $n = 4$ and $n = 6$ and large values of ϵ up to unity seem to work, but the numerical convergence is unreliable.

No satisfactory explanation can be offered for the difference between the solutions. It is difficult to see how the discontinuity at the origin for velocity (3.5) can alter the dynamo action so drastically. The iteration scheme may have crossed over to a different eigenvalue, but in several cases searches have been carried out for larger eigenvalues without success. The problem of maintenance of a field with a rope-like structure is a new one which needs more investigation.

When ϵ (or $n\epsilon$) was very small, positive growth rates could not be found (tables 8 and 9). Again numerical problems arise because the critical magnetic Reynolds numbers are so high, but for sufficiently large R_m, the growth rate should become positive.

When n is odd, the velocity defined by (3.1) gives the whole sphere a net angular velocity about the axis of symmetry. The field must be stationary in the frame of reference in which an appropriate weighted zonal velocity is zero. All such mean rotations must be zero for flows with n even because of the symmetry about the equator, but this is not the case when n is odd, and the field must therefore rotate.

Complex harmonics were used in the Bullard–Gellman expansions for the calculations carried

PHILOSOPHICAL TRANSACTIONS OF THE ROYAL SOCIETY A MATHEMATICAL, PHYSICAL & ENGINEERING SCIENCES

out when n is odd. The eigenvalues for $n = 3$ are complex, showing that the field does indeed rotate:

	R_m	σ	ω ($p = \sigma + i\omega$)
$n = 3, \epsilon = \frac{1}{10}$	10	−11.66	0.53
	20	−6.89	0.89
	40	8.57	1.43

It is possible to construct motions which have rotating fields, but also have zero mean angular rotation because of symmetry about the equator. An example is

$$\boldsymbol{u} = \epsilon \boldsymbol{S}_1 + \boldsymbol{T}_2. \tag{4.3}$$

This has helicity of opposite signs in the upper and lower hemispheres, which would be physically realistic if these were cyclonic motions. These motions have bands of adjacent cells at the equator which have opposite helicity. This also occurs in some of Roberts' 'second-order' dynamos (G. O. Roberts 1969, 1970), for which the time constants are complex and dynamo waves occur. For two-dimensional motions dependent on x and y, these waves travel in the z-direction. For motions in a sphere dependent on r and θ, they must travel in the ϕ-direction giving a rotation.

The interaction diagrams (Bullard & Gellman 1954) are instructive here. A rotating solution must have for each spherical harmonic, both $\sin\phi$ and $\cos\phi$ dependence. For example, a rotating equatorial dipole may be written as the real part of

$$(\boldsymbol{S}_1^{1c} + \boldsymbol{S}_1^{1s})\, e^{i\omega t}$$

where $\boldsymbol{S}_1^{1c}$ is based on the (complex) radial function $S(r)$, and $\boldsymbol{S}_1^{1s}$ is based on $i\boldsymbol{S}(r)$. When n is even, each harmonic has either $\sin\phi$ dependence or $\cos\phi$ dependence but never both, and therefore the symmetry of the problem does not admit rotating solutions.

For motions such as (4.3), the interaction diagrams contains both sine and cosine dependent harmonics, and therefore rotating solutions are possible. Assuming that an α-effect is operating, the field will be an equatorial dipole $\boldsymbol{S}_1^{1c}$ accompanied by a quadrupole toroidal field $\boldsymbol{T}_2^{1c}$. The sense of rotation depends on the signs of α in each hemisphere. If α is positive in the upper hemisphere the field will rotate in one sense; if it is negative in the upper hemisphere it will rotate in the opposite sense. The two dynamos are related to each other by reflexion (helicity is a pseudoscalar).

The difficulty in doing calculations is to find suitable velocities which have a simple spherical harmonic form, similar to (3.1) but ones in which the helicity changes sign across the equator. The motion (4.3), based on $r^2 \sin 2\pi r \tanh 2\pi(1-r)$ with $\epsilon = \frac{1}{10}$, does not appear to work as a dynamo:

R_m	σ	ω
10	−15.25	0.23
20	−25.25	−4.23
30	−34.31	−6.63
40	−42.22	−8.09

although the eigenvalue is complex. The only dynamo of this sort that was found to work was:

$$\boldsymbol{u} = \epsilon \boldsymbol{S}_1 + \boldsymbol{T}_3$$

with four cells radially and $\epsilon = \frac{1}{30}$:

R_m	σ	ω
10	−11.43	0.24
20	−13.21	0.37
30	−11.87	0.92
40	−5.88	−2.10
50	2.39	−2.76

This is not a good example of this sort of dynamo because the cells for the poloidal motion do not correspond with the cells for the toroidal motion. However, it is an approximation to a dynamo with an α which changes sign. The field is mostly S_1^{1c} and T_2^{1c} as expected. The behaviour of the imaginary part is strange, it may be because of poor convergence. This model also has a net angular rotation, and it cannot be proved that the rotation of the field is not due to that.

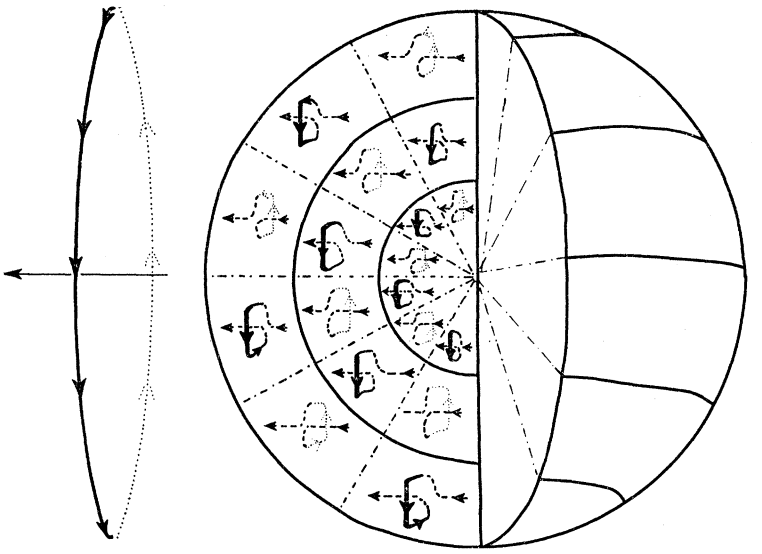

FIGURE 15. Field lines are pulled out and twisted by the motion. The field is initially uniform as shown to the left of the sphere. After reconnexion a toroidal field will be formed as shown.

It is now possible to account for the dynamo action of all the models reported here, on physical grounds. The field is regarded as being convected and distorted by the fluid motion. Consider an initial field line perpendicular to the axis of symmetry of the motion. The fluid motion, such as that of figure 2, will distort this field. Within any one cell of the motion, the field will be pulled out into loops in the ϕ-direction by the toroidal motion, and twisted by the poloidal motion. The result of this process is shown in figure 15. Thick lines indicate a field line in front of the paper. Reconnexion must occur at some point, when it does the new field will reinforce upwards in front of the paper and downwards behind it, except near the boundaries. The net result is something like the toroidal field shown at the left of the sphere. In figure 15 the field has been depicted as being twisted through a right angle for clarity. This is an oversimplification, but in any case the only directions in which the field can reinforce are those shown in the diagram.

The same mechanism will reproduce the original field from the toroidal field, completing a cycle from which the dynamo would be expected to work. It is two-step process, or to use the terminology of P. H. Roberts & Stix (1972) an 'α^2' dynamo.

When α is not uniform but changes sign across the equator, the situation is as shown in figure 16. The field will reinforce to give the T_2^1 harmonic. It is the behaviour near the equator which allows the field to rotate. At the equatorial plane there are two rows of cells with opposite helicity, as there are in some of the motions that give dynamo waves (G. O. Roberts 1969). It can be seen from figure 16 that the field at the equator can reconnect to contribute towards a dipole field in the direction out of the paper. This possibility of regenerating a dipole field perpendicular to the

original one is corroborated by the presence of this harmonic in the interaction diagram. With an axially symmetric velocity the choice of direction of the initial field is arbitrary, and therefore if a dipole field is produced perpendicular to the original one, a rotating solution must be possible.

5. Discussion

This work has shown that it is more profitable to search for fields which have an exponential time dependence than for steady fields. However, the method will be of less value when applied to problems with magnetic fields containing harmonics with more than a single order (in this case the harmonics were all of order one). For example a general rotating field cannot be represented by a single exponential in time. It may be that the dynamos of § 2 support time dependent fields which cannot be detected by the numerical method used.

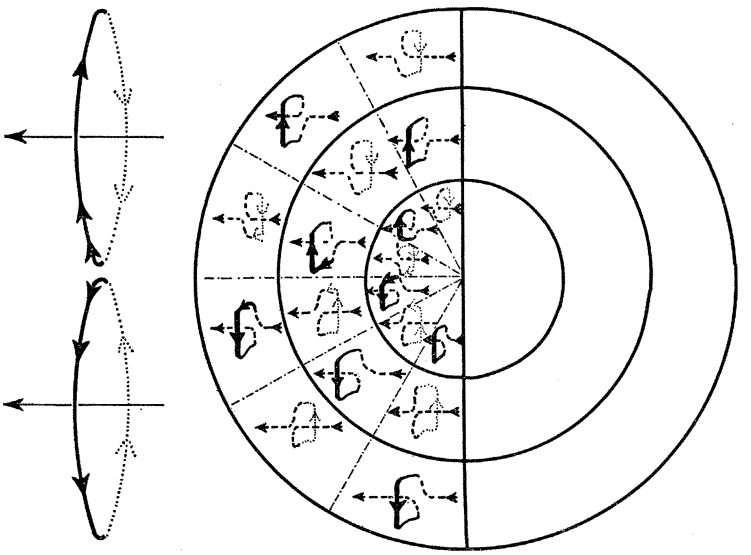

Figure 16. The advection of flux by a motion for which the helicity has different signs in the upper and lower hemispheres. The field will reconnect to form a $\boldsymbol{T}_2^1$ harmonic as shown to the left of the sphere. It can be seen that in the equatorial plane a field may be produced perpendicular to the original field. This is substantiated by the interaction diagram, in which the $\boldsymbol{S}_1^{1c}$ harmonic interacts with the $\boldsymbol{S}_1^{1s}$ harmonic.

Some of the solutions for the field in § 3 and 4 closely resemble spherical Bessel functions. This suggests that Bessel functions may be preferable to grid points in representing the radial variation of the field as originally suggested by Elsasser (1946*a*). In general this would destroy the banded structure of the matrix, but for some specific fluid motions the matrix may be made sparse.

The work of § 3 is related to that of Frazer (1971) who studied some models of the form:

$$\boldsymbol{u} = \epsilon \boldsymbol{S}_2 + \boldsymbol{T}_2.$$

However, his motions only had one cell in the radial direction, and like the one reported in § 3, did not sustain magnetic fields.

The axially symmetric dynamos may be rotated through $\frac{1}{2}\pi$ to make the magnetic field predominantly axially symmetric about $\theta = 0$. The velocity becomes symmetric about an axis in the equatorial plane. The spherical harmonic flow

$$u = \boldsymbol{S}_2^2 + \boldsymbol{T}_2^2$$

can be generated from $S_2 + T_2$ in this way. The field has dominant harmonics S_1 and T_1. Pekeris (1972, personal communication), has recently studied such a dynamo model.

The author wishes to thank his research supervisor, Sir Edward Bullard, F.R.S., for his help and encouragement, and Dr G. O. Roberts for a stimulating discussion and for advising him on the use of this method for finding eigenvalues of matrices. Most of the calculations were carried out on the IBM 360/44 computer at the Institute of Theoretical Astronomy, Cambridge, and thanks are due to Mr N. J. Butler and his staff for providing such an efficient service. The work was supported by a Research studentship from the Natural Environment Research Council.

References

Albasing, E. L., Bell, R. J. & Cooper, J. R. A. 1963 Report Ma 49, National Physical Laboratory.
Backus, G. E. 1958 *Annals Phys.* **4**, 372.
Braginskĭi, S. I. 1964 *Geomagn. Aeron.* **4**, 572.
Braginskĭi, S. I. 1965 *Soviet Phys. JETP* **20**, 726.
Bullard, E. C. & Gellman, H. 1954 *Phil. Trans. R. Soc. Lond.* A **247**, 213.
Childress, S. 1967 Course lectures. *Woods Hole Oceanographic Institute Summer School in Geophysical Fluid Dynamics*, p. 165.
Childress, S. 1970 *J. Math. Phys.* **11**, 3036.
Cowling, T. G. 1934 *Mon. Not. astr. Soc.* **94**, 39.
Elsasser, W. M. 1946*a* *Phys. Rev.* **69**, 106.
Elsasser, W. M. 1946*b* *Phys. Rev.* **70**, 202.
Elsasser, W. M. 1947 *Phys. Rev.* **72**, 821.
Frazer, M. C. 1971 Unpublished Ph.D. Thesis, Cambridge.
Gibson, R. D. & Roberts, P. H. 1967 In *Magnetism and the cosmos* (ed. W. R. Hindmarsh, F. J. Lowes, P. H. Roberts and S. K. Runcorn). New York: Wiley Interscience.
Gibson, R. D., Roberts, P. H. & Scott, S. 1969 In *The application of modern physics to the earth and planetary interiors.* (ed. S. K. Runcorn). New York: Wiley Interscience.
Gubbins, D. 1972 Unpublished Ph.D. Thesis, Cambridge.
Herzenberg, A. 1958 *Phil. Trans. R. Soc. Lond.* A **250**, 543.
Isaacson, E. & Keller, H. B. 1966 *Analysis of numerical methods.* New York: Wiley.
James, R. W. 1972 Submitted to *Proc. R. Soc. Lond.* A.
Krause, F. & Steenbeck, M. 1967 *Z. Naturforsch.* **22***a*, 671.
Lilley, F. E. M. 1970 *Proc. R. Soc. Lond.* A, **316**, 153.
Moffatt, H. K. 1970 *J. Fluid Mech.* **44**, 705.
Parker, E. N. 1955 *Astrophys. J.* **122**, 293.
Parker, E. N. 1971 *Astrophys. J.* **163**, 255.
Parker, R. L. 1966 *Proc. R. Soc. Lond.* A, **291**, 60.
Roberts, G. O. 1969 In *The application of modern physics to the earth and planetary interiors* (ed. S. K. Runcorn). New York: Wiley Interscience.
Roberts, G. O. 1970 *Phil. Trans. R. Soc. Lond.* A **266**, 535.
Roberts, G. O. 1972 *Phil. Trans. R. Soc. Lond.* A **271**, 411.
Roberts, P. H. 1967 *An introduction of magnetohydrodynamics.* London: Longmans,
Roberts, P. H. 1971 In *Lectures in applied mathematics* (ed. W. H. Reed). Providence: American Math. Soc.
Roberts, P. H. 1972 *Phil. Trans. R. Soc. Lond.* A, **272**, 663.
Roberts, P. H. & Stix, M. 1972 To appear in *Astronomy and astrophysics.*
Soward, A. M. 1971 *J. Math. Phys.* **12**, 2052.
Soward, A. M. 1972 *Phil. Trans. R. Soc. Lond.* A **272**, 431.
Steenbeck, M. & Krause, F. 1969*a* *Astr. Nachr.* **291**, 49.
Steenbeck, M. & Krause, F. 1969*b* *Astr. Nachr.* **291**, 271.
Steenbeck, M., Krause, F. & Rädler, K. H. 1966 *Z. Naturforsch.* **21***a*, 369.
Tough, J. G. 1967 *Geophys. J. R. astr. Soc.* **13**, 393.
Weiss, N. O. 1966 *Proc. R. Soc. Lond.* A **293**, 310.
Wilkinson, J. H. 1965 *The algebraic eigenvalue problem.* Oxford: Clarendon Press.
Zmuda, A. J. (editor) 1971 *World Magnetic Survey* 1957–1969. IAGA Bull. 28, IUGG Publication Office.

PHILOSOPHICAL TRANSACTIONS OF THE ROYAL SOCIETY A MATHEMATICAL, PHYSICAL & ENGINEERING SCIENCES